Advanced Powder Materials 3 (2024) 100189

Contents lists available at ScienceDirect

Advanced Powder Materials

journal homepage: www.keaipublishing.com/en/journals/advanced-powder-materials

Revealing the solid-state reaction process among multiphase multicomponent ceramic during ablation

Ziming Ye [a,b], Yi Zeng [a,*], Xiang Xiong [a,**], Sen Gao [a], Chen Shen [c], Shiyan Chen [a], Tianxing Jiang [a], Ge Yang [a]

[a] State Key Laboratory of Powder Metallurgy, Central South University, Changsha 410083, China
[b] International Institute for Material Innovation, Nanchang University, Nanchang 330031, China
[c] Institute of Materials Science, Technical University of Darmstadt, Darmstadt 64287, Germany

ARTICLE INFO

Keywords:
Multiphase ceramic
Multicomponent UHTCs
Solid-state reaction
Ablation resistance
Thermodynamic stability

ABSTRACT

Multiphase design is a promising approach to achieve superior ablation resistance of multicomponent ultra-high temperature ceramic, while understanding the ablation mechanism is the foundation. Here, through investigating a three-phase multicomponent ceramic consisting of Hf-rich carbide, Nb-rich carbide, and Zr-rich silicide phases, we report a newly discovered solid-state reaction process among multiphase multicomponent ceramic during ablation. It was found that this solid-state reaction occurred in the matrix/oxide scale interface region. In this process, metal cations are counter-diffused between the multicomponent phases, thereby resulting in their composition evolution, which allows the multicomponent phases to exist stably under a higher oxygen partial pressure, leading to the improvement of thermodynamic stability of three-phase multicomponent ceramic. Additionally, this solid-state reaction process appears synergistic with the preferential oxidation behavior among the oxide scale in enhancing the ablation performance.

1. Introduction

Transition-metal carbides, diborides, nitrides, etc., are well applicable for thermal protection systems in aerospace and nuclear fields due to their ultra-high melting points [1,2]. However, notable limitations concerning oxidation resistance remain for these conventional binary ultra-high temperature ceramics (UHTCs). Such as ZrC and HfC, their vulnerable porous scales are less protective during oxidation, however, as for ZrB_2, rapid evaporation of boron oxides above 1200 °C often leads to a premature failure of ceramic [3–6]. Therefore, several multiphase UHTCs systems such as ZrB_2–SiC [7] and ZrC–SiC [8] are developed and exhibited to improve oxidation or ablation resistance. Nonetheless, further examination under more aggressive conditions reveals that their performance is still insufficient to meet the increasing demand for the thermal protection of future propulsion systems, hypersonic vehicles, etc [2].

Inspired by high entropy alloys (HEAs), high entropy ceramics (HECs) are developed in recent years, and have been further extended to medium-entropy and non-equimolar compositions [9–11]. These novel multicomponent ceramics contain four or more different cations or anions expressing a blend of highly enhanced properties in physics and chemistry [12–14]. Notably, the remarkable enhancement in oxidation resistance of multicomponent UHTCs, for instance, $Hf_{0.2}Zr_{0.2}Ta_{0.2}Nb_{0.2}Ti_{0.2}C$ [15], $Hf_{0.25}Ta_{0.25}Zr_{0.25}Nb_{0.25}C$ [16], $Hf_{1/3}Zr_{1/3}Ti_{1/3}C$ [17], and $Zr_{0.8}Ti_{0.2}C_{0.74}B_{0.26}$ [18], was validated by researchers. As indicated earlier, the multiphase approach has been successfully applied to improve the oxidation and ablation resistance of conventional binary UHTCs. This motivates us to explore the novel multiphase multicomponent UHTCs.

To date, knowledge gaps remain with respect to the ablation mechanisms of multiphase multicomponent ceramics. Preliminary investigations have shown that thermodynamic factors play a vital role in the oxidation behavior and performance of single-phase multicomponent ceramics. For instance, driven by the differences in the relative thermodynamic favorability of oxides of Hf, Zr, and Ti, Hf/Zr would be preferentially oxidized in carbide containing Hf–Zr–Ti [19–21]. However, extending the system to multiphase multicomponent ceramics may cause a more complex reaction process during ablation. For instance, although it is generally believed that the constituent phases among conventional

* Corresponding author.
** Corresponding author.
E-mail addresses: zengyi001@csu.edu.cn (Y. Zeng), xiongx@csu.edu.cn (X. Xiong).

https://doi.org/10.1016/j.apmate.2024.100189
Received 28 January 2024; Received in revised form 28 February 2024; Accepted 6 March 2024
Available online 15 March 2024

multiphase UHTC would not react with each other under high temperatures [22,23], possible solid-state reaction might occur between the multicomponent phases of the multiphase multicomponent UHTC system. Unfortunately, these mechanisms are largely unexplored. These remaining knowledge gaps may hinder the design and optimization of multiphase multicomponent UHTCs.

In this work, a three-phase multicomponent ceramic, Hf–Zr–Ti–Nb–C–Si, consisting of Hf-rich carbide, Nb-rich carbide, and Zr-rich silicide phases, was fabricated. The ablation behavior was investigated, combining thermodynamic analysis, and the solid-state reaction between different multicomponent phases during ablation was revealed. Moreover, the composition and structure evolution of the multicomponent phases induced by solid-state reaction were elucidated. Importantly, its favorable impact and synergy with the preferential oxidation in the enhanced ablation performance were also systematically analyzed. In a broader context, this work suggests that multiphase design allows the multicomponent ceramic to achieve even better ablation performance, and it is worthwhile to explore.

2. Results and discussion

2.1. Microstructure and composition of the multiphase multicomponent ceramic

The microstructure of the multiphase multicomponent ceramic is shown in Fig. 1a. It can be seen from the polished cross-section that spherical white phases are uniformly distributed in some grey phases. Meanwhile, the evident distinction in the composition of these phases was confirmed by the EDS results (Fig. 1b and g): the spherical white phases are mainly composed of C and Hf, while the surrounding light grey phases are rich in Nb, and the dark grey phases are rich in Si and Zr. The HRTEM analyses (Fig. 1c–e) show that the spherical white phases can be indexed to f.c.c. carbide (HfC, JCPDS 65–8748), while the SAEDs of light and dark grey phases can be indexed to hexagonal carbide (Nb_2C, JCPDS 15–0147) and hexagonal silicide (Zr_5Si_3, JCPDS 06–0582), respectively. This appears to be consistent with the XRD analysis (Fig. 1f), and the phase-volume ratio of the Hf-rich carbide (P1), Nb-rich carbide (P2), and silicide (P3) phase is determined as 72.4 : 13.5: 14.1, respectively, from the XRD calculation. And the weight percentage of these phases is 72.19 wt%, 18.21 wt%, and 9.6 wt%, respectively. Combining the EPMA point analysis results (Table 1 and S1), the compositions of spherical white phase, light grey phase, and dark grey phase can be defined as $Hf_{0.65}Zr_{0.28}Ti_{0.04}Nb_{0.03}C$ (labeled as Hf-rich carbide), $(Nb_{0.46}Ti_{0.01}Hf_{0.31}Zr_{0.22})_2C$ (labeled as Nb-rich carbide), and $(Zr_{0.41}Hf_{0.34}Nb_{0.19}Ti_{0.06})_5Si_3$ (labeled as Zr-rich silicide), respectively. Moreover, the SEM- and STEM-EDS mapping results also confirm the uniform elemental distribution in each phase in micro- and nano-scale (Fig. 1b and S1).

2.2. The overall structure and composition after ablation

During ablation, the multiphase multicomponent ceramic achieved a surface temperature of 2550 K, which is similar to that of single-phase multicomponent carbide $Hf_{0.50}Zr_{0.30}Ti_{0.10}Nb_{0.10}C$ under identical test conditions [24]. As shown in Fig. 2a, the multiphase multicomponent ceramic demonstrates a superior ablation resistance. Its MAR is 13 times lower than that of its single-phase counterpart and is 3 orders of magnitude lower than that of conventional ZrC material. However, the LAR of multiphase multicomponent ceramic is quite close to that of its single-phase counterpart, and it is lower than that of $Hf_{0.2}Zr_{0.2}Ti_{0.2}Nb_{0.2}Ta_{0.2}C$-20 vol% SiC which was ablated under a much lower heat flux (4.18 MW m^{-2}) [25], implying a good dimensional stability during ablation. As shown in the macroscopic image of the ablated samples, the ablation center of the multiphase multicomponent ceramic is relatively smoother and more intact than that of the single-phase counterpart (Fig. 2b). The SEM observation reveals a consistent result (Fig. 2e).

A set of peaks corresponding to the monoclinic HfO_2 (JCPDS cards 43–1017) was detected in the XRD patterns of the ablated surface (Fig. 2g), this suggests that the as-formed oxide scale is mainly composed of Hf-rich oxide. In addition, despite small amounts of SiO_2 remaining within the inner oxide scale (Fig. 2f), its diffraction peaks are not

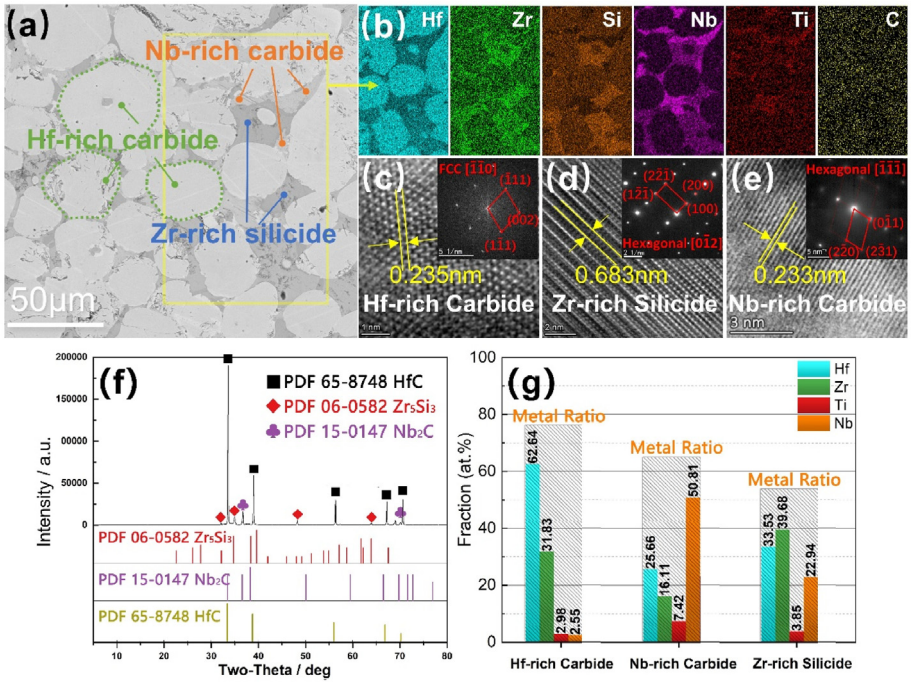

Fig. 1. (a) SEM image of a polished cross-section of multiphase multicomponent ceramic. (b) EDS mapping of the corresponding region in Fig. 1a; (c–e) HRTEM images of Hf-rich carbide phase (c), Zr-rich silicide phase (d) and Nb-rich carbide phase (e) with FFT patterns and SAEDs inset, respectively; (f) XRD patterns of the multiphase multicomponent ceramic; (g) EDS point analysis of the metal ratio of each ceramic phase.

Table 1
The compositions of the constituent phases obtained by EPMA.

Phase	Phase 1 (Hf-rich carbide)	Phase 2 (Nb-rich carbide)	Phase 3 (Zr-rich silicide)
Composition	$Hf_{0.65}Zr_{0.29}Ti_{0.04}Nb_{0.02}C$	$(Nb_{0.46}Ti_{0.01}Hf_{0.31}Zr_{0.22})_2C$	$(Zr_{0.41}Hf_{0.34}Nb_{0.19}Ti_{0.06})_5Si_3$

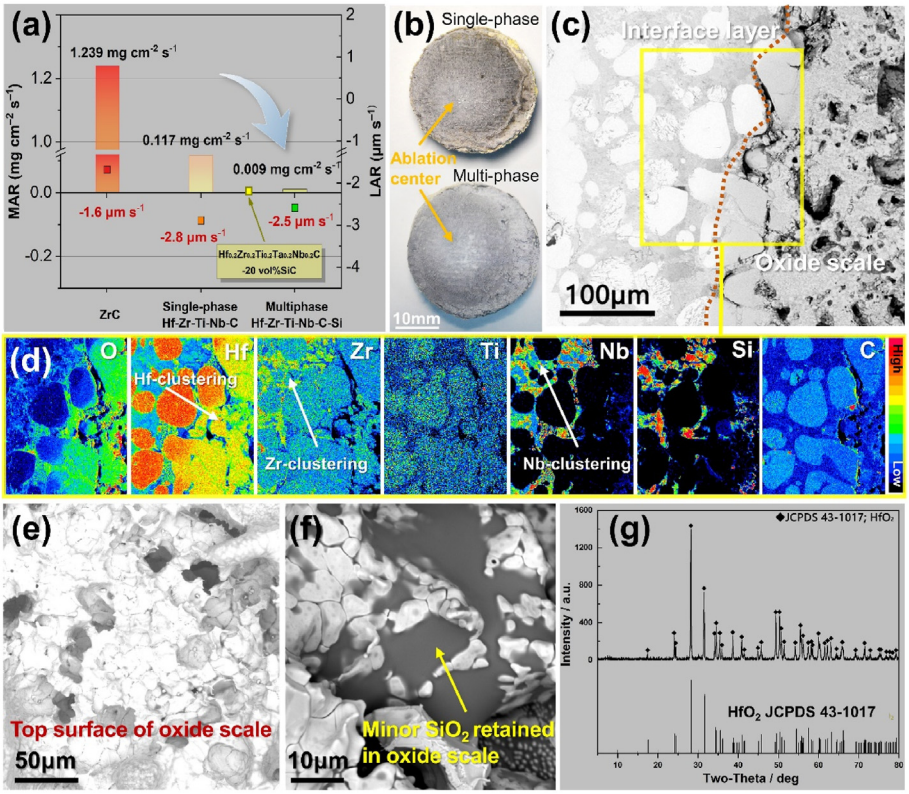

Fig. 2. (a–b) Comparisons of ablation performance (a) and macroscopic ablation morphology (b) (the data of $Hf_{0.50}Zr_{0.30}Ti_{0.10}Nb_{0.10}C$ and $Hf_{0.2}Zr_{0.2}Ti_{0.2}Nb_{0.2}Ta_{0.2}C$-20 vol% SiC are referred to the prior work [24,25]); (c) Cross-section morphology of the central ablated area; (d) Elemental distribution of the matrix/oxide scale interface obtained via EPMA; (e–f) SEM image of the top surface of the scale (e) and the as-formed SiO_2 retained in the oxide scale (f); (g) XRD patterns of the ablated sample.

observed in the XRD patterns, which means most of the Si-component is oxidized into gaseous products. It is, therefore, not expected that the small amounts of as-formed glassy SiO_2 will provide a significant advantage in reducing the ablation rate. However, elemental segregation was detected at the interface between the ceramic matrix and oxide layer (Fig. 2c and d), particularly the Hf-enrichment in the whole oxide scale. This is evidenced by the aforementioned XRD analysis. Meanwhile, the Zr-/Nb-clustering among the matrix/oxide scale interface is also observed (Fig. 2c and d). Importantly, these composition evolutions together with the unique underlying ablation mechanism may be responsible for enhancing the ablation performance.

2.3. *Structural and compositional evolution of matrix/oxide scale interface region*

To investigate the unique ablation mechanism of multiphase multicomponent ceramic, a thin TEM slice was lifted out from a triple junction area among the matrix/oxide scale interface region (Fig. 3a, yellow box) and then analyzed by TEM. The HAADF image (Fig. 3b) demonstrates the morphology of the triple junction area. Three phases were observed (Fig. 3b–d). Notably, an intermediate phase (labeled as IP1) formed among the Hf-rich carbide (Fig. 3a and b). According to the Zr and O elemental mapping results (Fig. 3d), the magnified STEM-EDS (Fig. 3f) and HRTEM analysis (Fig. S2), this IP1 phase can be determined as Zr-rich oxide. Interestingly, similar Zr-rich oxide intermediate phases were also detected among Zr-rich silicide (Fig. 3e) and Nb-rich carbide phases (Fig. 3g). These observations can be substantiated by the corresponding STEM-EDS point analysis (Fig. 3c) and the further HRTEM analysis of these phases (Figs. S3 and S4).

It is noted that these observations reveals a mismatch with the thermodynamic prediction with respect to preferential oxidation [19,20]. Given both the experimental observation and thermodynamic calculations show that Hf would be preferentially oxidized in multicomponent carbide and silicide systems and yield Hf-rich oxide [24,26], the observed oxides here are Zr-enriched. This mismatch strongly suggested that there are some undiscovered oxidation mechanisms of multiphase multicomponent ceramics. In addition, although the crystal structure of residue primary phases remains unaltered (Figs. S2–4b), significant compositional evolution has occurred: the residue Hf-rich carbide becomes Zr-rich, while the remarkable enrichment of Nb in residue Nb-rich carbide and Zr-rich silicide phases was also detected (Fig. 5d and Table 2). These observations are in good agreement with the observed composition evolutions shown in 2.2. More importantly, further study on their implications for ablation performance is required.

2.4. *Structural and compositional evolution of oxide scale*

Similarly, TEM analysis was also performed on a triple junction area among the oxide scale (the red box in Fig. 4a) to investigate its structural and compositional evolution. As depicted in the HAADF image (Fig. 4b) and the corresponding STEM-EDS mapping (Fig. 4d), Hf-rich oxides becomes the main oxidation products. For instance, micron-sized monoclinic Hf-rich oxides (labeled as OP4-6, detailed analyses were presented in Figs. S6–8) forms at the phase boundaries of Hf-rich carbide, Nb-rich carbide and Zr-rich silicide phases (Fig. 4b–e, f), while, some Hf-rich oxides also forms among Hf-rich carbide (Fig. S5) and Zr-rich silicide

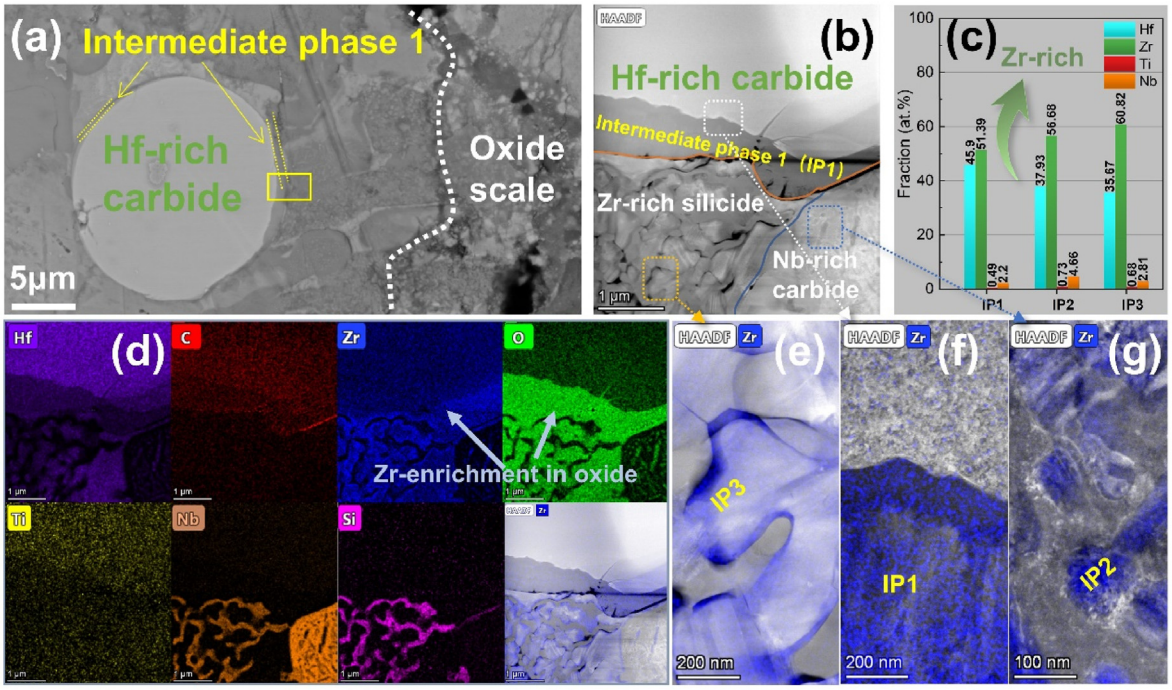

Fig. 3. (a) The exact position (yellow box) where the TEM slice lifted out; (b) HAADF image of TEM sample 1; (c–d) STEM-EDS point analysis results (c) and elemental mapping (d) of the oxides derived from each phase; (e–g) The magnified HAADF image of the oxides derived from Zr-rich silicide phases (e), Hf-rich carbide (f), and Nb-rich carbide (g), respectively, with EDS Zr map layered.

Table 2
Phase composition before and after the initial oxidation via EDS.

Phases	Initial oxidation product	Residue primary phase
Compositions	$Zr_{0.51}Hf_{0.46}Nb_{0.02}Ti_{0.01}O_2$ (IP1)	$Hf_{0.53}Zr_{0.42}Ti_{0.01}Nb_{0.04}C$
	$Zr_{0.56}Hf_{0.38}Nb_{0.05}Ti_{0.01}O_2$ (IP2)	$(Nb_{0.77}Zr_{0.08}Hf_{0.12}Ti_{0.03})_2C$
	$Zr_{0.61}Hf_{0.35}Nb_{0.03}Ti_{0.01}O_2$ (IP3)	$(Nb_{0.81}Zr_{0.14}Hf_{0.04}Ti_{0.01})_5Si_3$

phases (Fig. 4 f). This significant tendency of Hf enrichment was confirmed by the corresponding STEM-EDS point analysis (Fig. 4c). Meanwhile, the crystal structure of these oxides was determined by further HRTEM analysis (Figs. S5–8), which is consistent with the abovementioned analysis.

In summary, the oxide scale demonstrates an oxidation reaction regime different from that of matrix/oxide scale interface, specifically, it conforms to the reaction regime of preferential oxidation of Hf. Generally, an oxygen activity gradient would develop across the material during ablation [27], which means the exterior region (i.e., the oxide scale) usually possesses a higher oxygen partial pressure pO_2 than the matrix/oxide scale interface, and experiences higher extent of oxidation. It is thus inferred that the pO_2 might alter the oxidation reaction regime of the multiphase multicomponent UHTC.

2.5. The ablation mechanism of the multiphase multicomponent ceramic

To probe into the potential ablation mechanism, thermodynamic software Factsage 8.2 was used to perform the equilibrium calculations of oxidation of the multiphase multicomponent ceramic. Due to the absence of thermodynamic data of complex solid solutions, a simplified example of multiphase system $HfZrC_2$-$NbHfC_2$-$ZrHfSi_2$ was selected for analyzing the reaction trend according to the main components of the multiphase multicomponent ceramic. In addition, in order to describe the relatively low pO_2 of the matrix/oxide scale interface, the input of the O_2 of the thermodynamic calculations was limited to 3 mol [20].

The equilibrium calculation results (Table 3), reveals that the Hf-component is preferentially oxidized, and HfO_2 is the main oxidation product in this system. More significantly, an intermediate phase, Zr-rich carbide (i.e., $Zr_{0.57}Nb_{0.25}Hf_{0.18}C_{0.95}$), was predicted to form through the solid-state reaction of phases. Meanwhile, the Zr/Hf-rich silicide becomes Nb-rich during this solid-state reaction (i.e., $Nb_{0.1}Hf_{0.1}Zr_{0.06}C_{0.95}$). Notably, this predicted Zr- and Nb-enrichment in residue carbide together with the Nb-enrichment in residue silicide is in good agreement with experimentally observed composition evolutions (Fig. 5d). These results suggests that the oxidation behavior of multiphase multicomponent system involves the solid-state reaction of phases and the preferential oxidation of thermodynamically favored components.

However, the equilibrium calculation results are not perfectly consistent with the experimental observations. For instance, the observed Zr-rich intermediate phases which formed among the matrix/oxide scale interface are Zr-rich oxides rather than the predicted Zr-rich carbide (i.e., $Zr_{0.57}Nb_{0.25}Hf_{0.18}C_{0.95}$). This mismatch implies that, during ablation, the solid-state reaction and the preferential oxidation reaction occur synchronously. And, it can be inferred from the enrichment of Zr in the oxide that the solid-state reaction, which yields Zr-rich phases, prevailed over the preferential oxidation reaction among the matrix/oxide scale interface. The chemical equation of the solid-state reactions together with partial oxidation is provided in the Supplementary Material.

Based on the Wagner reaction mechanism and related research [28, 29], the solid-state reaction of different phases is achieved by the interdiffusion of cations. As a result, the intermediate phase would form at the phase boundary (i.e., the grain boundary) [29]. In this work, according to the predicted composition evolution of residue carbide and silicide phases (Table 3), it can be thus inferred that the interdiffusion of Nb and Zr would occur among the phase boundary of carbide and silicide during solid-state reaction (Fig. 5b). Interestingly, the phase boundary also provided space for oxidation reactions due to oxygen diffusion always occurring along the grain boundaries (Fig. 5b). While, the tendency of preferential oxidation would promote the migration of preferentially oxidized components (i.e., Hf) to the region where oxidation occurs [24]. Since the solid-state reaction prevailed over the preferential oxidation reaction among the matrix/oxide scale interface, the Nb–Zr

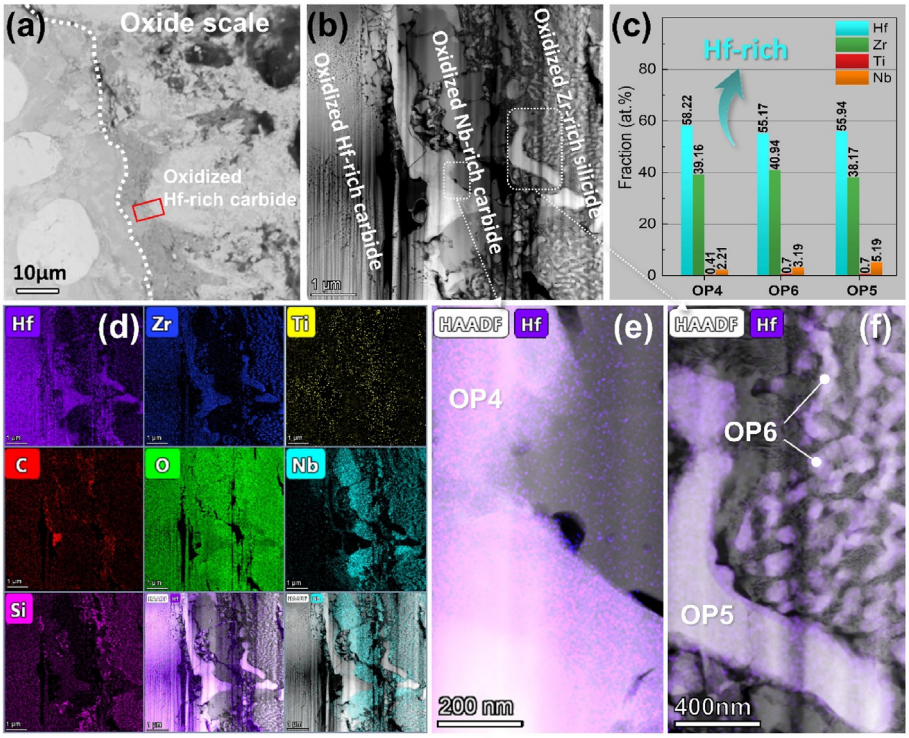

Fig. 4. (a) The position (red box) where the TEM slice lifted out; (b) HAADF image of TEM sample; (c–d) STEM-EDS point analysis results (c) and elemental mapping (d) of the oxides derived from each phase; (e–f) The magnified HAADF image of the oxides derived from Hf-rich carbide, Nb-rich carbide, and Zr-rich silicide phases, respectively, with EDS Hf map layered.

interdiffusion caused by the solid-state reaction dominated this reaction process, rather than the migration of preferentially oxidized component (i.e., Hf) due to the preferential oxidation reaction. Notably, in this process, the diffusion coefficient of Nb-diffusion from carbide is believed to be several magnitudes lower than that of Zr-diffusion from the Zr-rich silicide [30,31]. Thus, Zr became the dominant diffusion species. As a result, Zr-rich intermediate phases formed. Since oxygen continues to diffuse to this matrix/oxide scale, the as-formed Zr-rich carbide intermediate phases were subsequently oxidized into Zr-rich oxide.

Likewise, the thermodynamic analysis results and the above analysis concerning the cations diffusion are also applicable to the interpretation of the oxidation reaction regime of the oxide scale. As indicated earlier, the ablation of the multiphase system involved two parallel competition reactions, namely, the solid-state reaction of phases and the preferential oxidation of thermodynamically favored elements. More importantly, the competition would be primarily affected by the pO_2. It can be thus inferred that, due to the higher local pO_2 of the oxide scale region, the preferential oxidation reaction prevailed over the solid-state reaction and became the dominant reaction. Thus, the migration of Hf to the region where oxidation occurs should be preferred (Fig. 5c). As a result, Hf-rich oxides became the main oxidation products. In summary, the composition difference between the oxidation products of the oxide scale and the matrix/oxide scale interface region is interpreted from the transition in the reaction regime. While, the mismatch with the thermodynamic prediction with respect to the preferential oxidation is also rationalized.

2.6. Impact on the ablation performance

After the solid-state reaction, the composition evolutions among the matrix/oxide scale interface region would definitely impact the ablation performance. Fundamentally, the solid-state reaction was driven by the free energy minimization, which means the free energy of the multiphase multicomponent system was lowered by the composition evolutions, and the thermodynamic stability of the multicomponent carbide and silicide phases should be improved. Here, the predominance diagrams of MC/MSi + O_2 systems (e.g., M = Hf, Zr, Ti, Nb) were applied to assist the interpretation of the variation in thermodynamic stability. These diagrams illustrate the stable ranges of carbide/silicide phases (*i.e.,* edges of color blocks showed in Fig. 5e and f). As shown in Fig. 5d, the residue Hf-rich carbide became Zr-rich, while, the remarkable enrichment of Nb in residue Nb-rich carbide and Zr-rich silicide phases was also detected. Comparing the stable ranges of Hf- and Zr- carbide, it is found that the carbide of Zr possesses the broader stable range around the ablation temperature. It can also be inferred that the stable ranges of Nb-carbide/silicide are significantly greater than that of Zr-carbide/silicide. This suggests that, the composition evolution (Fig. 5d) allowed the multicomponent phases to exist stably under a higher oxygen partial pressure (Fig. 5e and f), which led to the improvement of thermodynamic stability of three-phase multicomponent ceramic. This would enhance the ablation performance of the material within a specific temperature range. Nonetheless, it should be noted that the oxidation products of Nb and Si might deteriorate the ablation performance under the higher temperatures.

In addition, the structural and compositional evolution of the oxide scale also contributes to the enhancement of ablation performance. Due to the preferential oxidation of Hf, Hf-rich oxides became the main oxidation products. More importantly, in this process, the oxides of preferentially oxidized Hf among carbide and silicide phases would preferentially nucleate and further constitute a Hf-rich oxide skeleton (Figs. S5a and 8a). It could sustain an adherent high-melting oxide scale during ablation [32]. Furthermore, the laggingly oxidized Nb would form the infilling oxides of the Hf-rich skeleton, and the melting phase formed by the Nb-/Si-oxides could seal the pores and defects, making this oxide layer relatively impervious and stable (Fig. S8a). Generally, this self-healing structure is desirable for better protective performance. A more detailed discussion is given in the previous works [24]. Summarizing, the synergisms of the solid-state reaction and preferential oxidation were critical in the enhancing the ablation performance. More broadly,

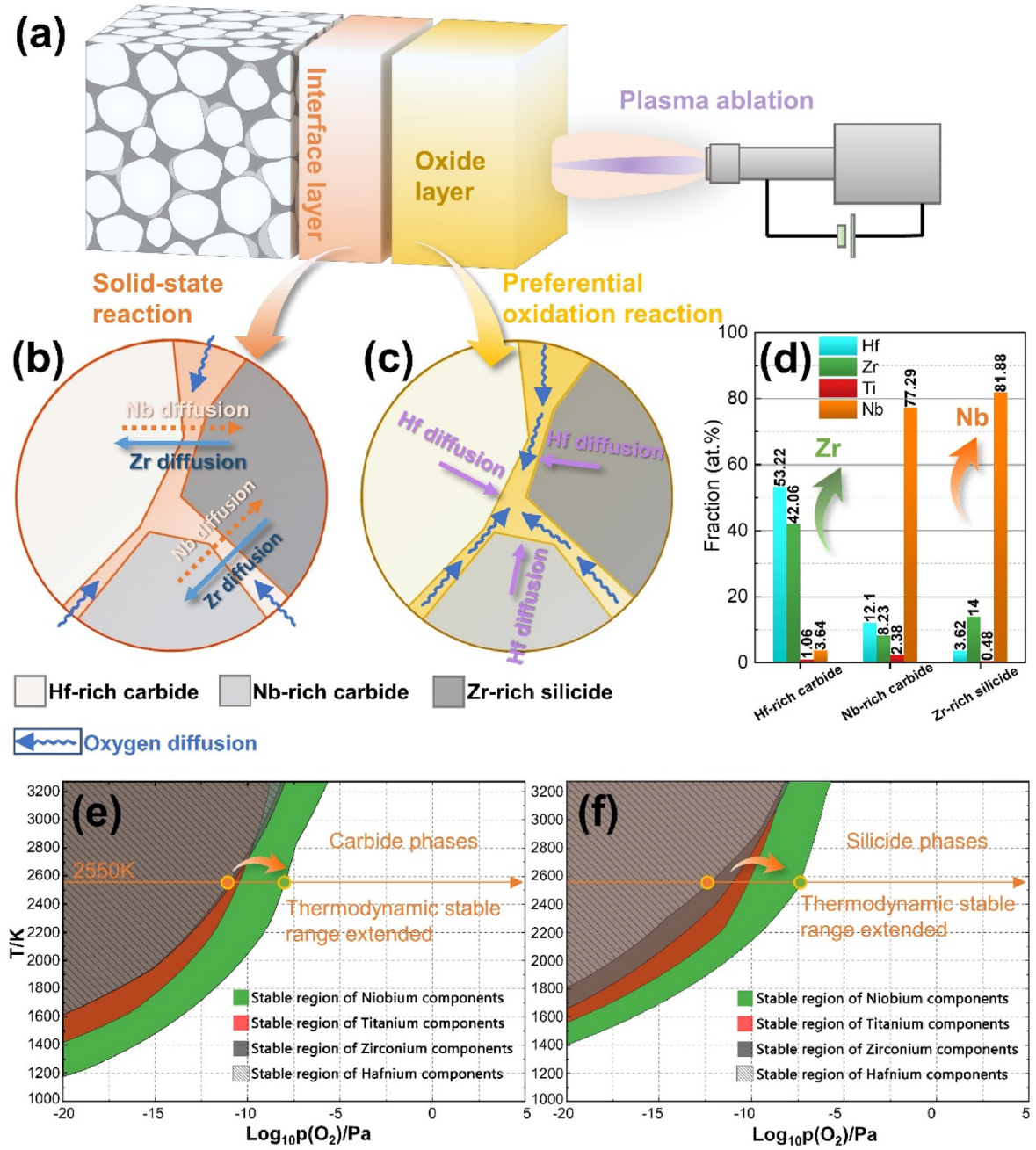

Fig. 5. (a–c) Schematic diagram of the ablation mechanism of multiphase multicomponent ceramic (a) including the solid-state reaction among the matrix/oxide scale interface (b) and the preferential oxidation among the oxide layer (c); (d) The composition of carbide and silicide phases after solid-state reaction obtained by STEM-EDS point analysis; (e–f) Comparison of the stable range of MC carbides (e) and MSi silicides (f) (e.g., M=Hf, Zr, Ti, Nb, the separate predominance diagrams of MC and MSi are shown in Fig. S9, and they can be referred to our previous works ref. [24,26]).

Table 3
Equilibrium calculations of the $HfZrC_2$-$NbHfC_2$-$ZrHfSi_2$ system during the initial stage of oxidation. The input of oxygen is 3 mol, and the temperature is 2550 K.

	Constituents		
Reactants	$HfZrC_2$ (cr)	$NbHfC_2$ (cr)	$ZrHfSi_2$(cr)
Input (mol)	1	1	1
Products	HfO_2(cr)	$Zr_{0.57}Nb_{0.25}Hf_{0.18}C_{0.95}$(cr)	$Nb_{0.1}Hf_{0.1}Zr_{0.06}Si_{1.28}$(cr)
Output (mol)	2.2367	3.3248	1.7558

this work also reveals that multiphase design is a promising approach toward superior ablation performance of multicomponent UHTC. Moreover, thermodynamic pre-evaluation of the solid-state reaction and preferential oxidation could facilitate the multiphase design of multicomponent UHTC.

3. Conclusion

In this work, the solid-state reaction process among multiphase multicomponent ceramic during ablation was revealed through the investigations on the ablation behavior of a three-phase multicomponent

ceramic consisting of Hf-rich carbide, Nb-rich carbide, and Zr-rich silicide phases. It was found that this solid-state reaction occurred in the matrix/oxide scale interface region. In this process, metal cations is counter-diffused between the multicomponent phases. As a result, the compositions of these multicomponent phases are largely altered. More importantly, this composition evolution allows the multicomponent phases to exist stably under a higher oxygen partial pressure, which improves the thermodynamic stability of the three-phase multicomponent ceramic. In addition, the preferential oxidation of Hf among the oxide layer leads to a self-healing structure of Hf-rich oxide skeleton infilled with Nb-/Si-oxides, which enhances the integral protection performance against oxidizing environments. In conclusion, the synergism of solid-state reaction and preferential oxidation evidently enhances the ablation performance. More broadly, this work demonstrates that multiphase design is a promising approach toward superior ablation performance of multicomponent UHTC. Meanwhile, the present findings may provide a preliminary basis for the future development of multiphase multicomponent UHTCs.

4. Experimental section

4.1. The fabrication of the multiphase multicomponent ceramic

The multiphase multicomponent ceramic, Hf–Zr–Ti–Nb–C–Si, was prepared on a carbon/carbon (C/C) composite through reactive melt infiltration (RMI) method integrated with a thermal evaporation (TE) process. And some carbides were allowed to infiltrate into the C/C composite to decrease the risk of cracking during the plasma ablation test. During the fabrication process, the C/C composite (density: 1.00 g cm^{-3}) was embedded into the mixed metal powder with a composition of 55 at. % Hf-30 at. % Zr-5 at. % Ti-10 at. % Nb within a graphite crucible (46.5 mm in diameter and a height of 50 mm). And then put it into a big graphite crucible (65 mm in diameter and a height of 80 mm) containing silicon source. The Hf, Zr and Ti raw powders (d~40 μm, 99.2% purity) were purchased from Jinzhou Haixin Metal Materials Co., Ltd. China. Nb raw powder (d~45 μm, 99.95% purity) was purchased from Aladdin Scientific Corp. And silicon source (i.e., Si powder, d~45 μm, 99.99% purity, Aladdin Scientific Corp) was put in the big graphite crucible. The heat treatment was conducted by a resistance furnace During heat treatment, the temperature was firstly heated to 1873.15 K under a heating rate of 10 K/min and kept for 0.5 h. In this thermal evaporation stage, the pressure was maintained at 200 Pa. Then, the furnace was evacuated and heated to 2373.15 K to carry out the RMI process, the duration of this stage was 1 h. The multiphase multicomponent ceramic, Hf-Zr-Ti-Nb-C-Si, was formed in this process, and the formation mechanism has been discussed in the prior work [26].

4.2. Ablation test

In this work, the ablation test was carried out by a plasma torch device. During the test, the flow rates of argon and hydrogen gas were set as 2000 and 180 L h^{-1}, respectively. And the working current and voltage were set as 699 A and 64 V, respectively. The test sample (The sample was not polished), having a size of Ø30 mm × 10 mm, was fixed in a water-cooled copper holder, with a distance of 55 mm to the plasma gun tip. The temperature of the central ablation region sample was measured as ca.2550 K using an optical pyrometer. The heat flux of the plasma torch was measured to be 6.73 MW m^{-2} by a heat flux sensor (GD-B3-12 M, Beijing East Summit Tech. Inc.). The test duration was 120 s. The mass ablation rate (MAR) and linear ablation rate (LAR) were calculated by Eqs. (1) and (2), respectively:

$$\mathrm{LAR} = \frac{d_i - d_f}{t} \tag{1}$$

$$\mathrm{MAR} = \frac{m_i - m_f}{t} \tag{2}$$

Where t is the test duration (s), d_i (μm) and d_f (μm) are the initial and final thicknesses measured at the center of the samples, respectively; m_i (mg) and m_f (mg) are the initial and final mass of the samples, respectively; These values were measured by the electronic balance (±0.0001 g) and gauge (±0.01 mm) respectively. The results of LAR and MAR were averaged over three samples.

4.3. Characterization

The morphology of the sample was unanalyzed by a scanning electron microscope (SEM, TESCAN, MIRA4 LMH) combined with an energy dispersive spectroscopy (EDS, Ultam-Max-50), backscattered electrons (BSE) detector was used throughout this work. The element content and distribution were observed by an electron probe microanalysis system (EPMA, JEOL, Jxa8230). The phase structure was identified via the X-ray diffraction (XRD) analyzer (Bruker D8 ADVANCE) at a scanning speed of 0.5°·min^{-1} from 5° to 80°. High-resolution transmission electron microscope (HRTEM) images and High-angle annular dark field (HAADF) scanning transmission electron microscopy (STEM) images were obtained by Talos F200x (scanning) transmission electron microscope equipped with an EDS system. The accelerating voltage for TEM imaging and STEM was 200 kV. The spot size for TEM-EDS was set as 100 nm × 100 nm. TEM samples were processed by a focused ion beam (FIB, FEI Helios Nanolab 600i). The thermodynamic data and diagrams were calculated by the phase and equilibrium modules of FactSage 8.2, respectively.

Declaration of competing interest

The authors declare that they have no known competing financial interests or personal relationships that could have appeared to influence the work reported in this paper.

Acknowledgments

This work was supported by the National Natural Science Foundation of China (52072410 and 51602349). Yi Zeng is an editorial board member for Advanced Powder Materials and was not involved in the editorial review or the decision to publish this article. The authors declare that they have no known competing financial interests or personal relationships that could have appeared to influence the work reported in this paper.

Appendix A. Supplementary data

Supplementary data to this article can be found online at https://doi.org/10.1016/j.apmate.2024.100189.

References

[1] E. Wuchina, E. Opila, M. Opeka, B. Fahrenholtz, I. Talmy, UHTCs: ultra-high temperature ceramic materials for extreme environment applications, Electrochem. Soc. Interface 16 (4) (2007) 30–36.
[2] S.R. Levine, E.J. Opila, M.C. Halbig, J.D. Kiser, M. Singh, J.A. Salem, Evaluation of ultra-high temperature ceramics foraeropropulsion use, J. Eur. Ceram. Soc. 22 (14–15) (2002) 2757–2767.
[3] W.G. Fahrenholtz, Thermodynamic analysis of ZrB_2–SiC oxidation: formation of a SiC-depleted region, J. Am. Ceram. Soc. 90 (1) (2007) 143–148.
[4] W.G. Fahrenholtz, The ZrB_2 volatility diagram, J. Am. Ceram. Soc. 88 (12) (2005) 3509–3512.
[5] R.F. Voitovich, E.A. Pugach, High-temperature oxidation of ZrC and HfC, Sov. Powder Metall. Met. Ceram. 12 (1973) 916–921.
[6] L.Y. Zhao, D.C. Jia, X.M. Duan, Z.H. Yang, Y. Zhou, Oxidation of ZrC–30 vol% SiC composite in air from low to ultrahigh temperature, J. Eur. Ceram. Soc. 32 (4) (2012) 947–954.
[7] P. Hu, G.L. Wang, Z. Wang, Oxidation mechanism and resistance of ZrB_2–SiC composites, Corrosion Sci. 51 (11) (2009) 2724–2732.

[8] D. Pizon, L. Charpentier, R. Lucas, S. Foucaud, A. Maitre, M. Balat-Pichelin, Oxidation behavior of spark plasma sintered ZrC–SiC composites obtained from the polymer-derived ceramics route, Ceram. Int. 40 (3) (2014) 5025–5031.
[9] A.J. Wright, J. Luo, A step forward from high-entropy ceramics to compositionally complex ceramics: a new perspective, J. Mater. Sci. 55 (23) (2020) 9812–9827.
[10] J. Gild, Y.Y. Zhang, T. Harrington, S.C. Jiang, T. Hu, M.C. Quinn, W.M. Mellor, N.X. Zhou, K. Vecchio, J. Luo, High-entropy metal diborides: a new class of high-entropy materials and a new type of ultrahigh temperature ceramics, Sci. Rep. 6 (1) (2016) 37946.
[11] C.M. Rost, E. Sachet, T. Borman, A. Moballegh, E.C. Dickey, D. Hou, J.L. Jones, S. Curtarolo, J. Maria, Entropy-stabilized oxides, Nat. Commun. 6 (1) (2015) 8485.
[12] C. Oses, C. Toher, S. Curtarolo, High-entropy ceramics, Nat. Rev. Mater. 5 (2020) 295–309.
[13] R.Z. Zhang, M.J. Reece, Review of high entropy ceramics: design, synthesis, structure and properties, J. Mater. Chem. A 7 (39) (2019) 22148–22162.
[14] L. Feng, W.G. Fahrenholtz, D.W. Brenner, High-entropy ultra-high-temperature borides and carbides: a new class of materials for extreme environments, Annu. Rev. Mater. Res. 51 (2021) 165–185.
[15] B.L. Ye, T.Q. Wen, D. Liu, Y.H. Chu, Oxidation behavior of $(Hf_{0.2}Zr_{0.2}Ta_{0.2}Nb_{0.2}Ti_{0.2})C$ high-entropy ceramics at 1073-1473 K in air, Corrosion Sci. 153 (2019) 327–332.
[16] Y.C. Wang, R.Z. Zhang, B.H. Zhang, O. Skurikhina, P. Balaz, V. Araullo-Peters, M.J. Reece, The role of multi-elements and interlayer on the oxidation behaviour of (Hf–Ta–Zr–Nb)C high entropy ceramics, Corrosion Sci. 176 (2020) 109019.
[17] H.L. Lun, Y. Zeng, X. Xiong, Z.M. Ye, Z.W. Zhang, X.C. Li, H.K. Chen, Y. F Liu, Oxidation behavior of non-stoichiometric (Zr, Hf, Ti)C_x carbide solid solution powders in air, J. Adv. Ceram. 10 (2021) 741–757.
[18] Y. Zeng, D.N. Wang, X. Xiong, X. Zhang, P.J. Withers, W. Sun, M. Smith, M.W. Bai, P. Xiao, Ablation-resistant carbide $Zr_{0.8}Ti_{0.2}C_{0.74}B_{0.26}$ for oxidizing environments up to 3,000 °C, Nat. Commun. 8 (1) (2017) 15836.
[19] L. Backman, J. Gild, J. Luo, E.J. Opila, Part I: theoretical predictions of preferential oxidation in refractory high entropy materials, Acta Mater. 197 (2020) 20–27.
[20] L. Backman, J. Gild, J. Luo, E.J. Opila, Part II: experimental verification of computationally predicted preferential oxidation of refractory high entropy ultra-high temperature ceramics, Acta Mater. 197 (2020) 81–90.
[21] S.Y. Chen, Z.K. Chen, J.M. Wang, Y. Zeng, W.L. Song, X. Xiong, X.C. Li, T.Q. Li, Y.C. Wang, Insight into the effect of Ti substitutions on the static oxidation behavior of (Hf, Ti) C at 2500 °C, Adv. Powder. Mater. 3 (2) (2024) 100168.
[22] S.G. Chen, Y.Z. Gou, H. Wang, J. Wang, Fabrication and characterization of precursor-derived non-oxide ZrC–SiC multiphase ultrahigh temperature ceramics, J. Eur. Ceram. Soc. 36 (16) (2016) 3843–3850.
[23] F. Li, X. Huang, Preparation of highly porous ZrB_2/ZrC/SiC composite monoliths using liquid precursors via direct drying process, J. Eur. Ceram. Soc. 38 (4) (2018) 1103–1111.
[24] Z.M. Ye, Y. Zeng, X. Xiong, Q.B. Wen, H.L. Lun, Elucidating the role of preferential oxidation during ablation: insights on the design and optimization of multicomponent ultra-high temperature ceramics, J. Adv. Ceram. 11 (12) (2022) 1956–1975.
[25] W.J. Guo, J. Hu, Y.C. Ye, S.X. Bai, Ablation behavior of (TiZrHfNbTa)C high-entropy ceramics with the addition of SiC secondary under an oxyacetylene flame, Ceram. Int. 48 (9) (2022) 12790–12799.
[26] Z.M. Ye, Y. Zeng, X. Xiong, C.L. Xia, J.R. Hu, J.C. Zhang, J.L. Long, R. Li, The synergistic role of hierarchical preferential oxidation in the enhanced ablation performance of multi-phase multicomponent ultra-high temperature ceramics, J. Eur. Ceram. Soc. 43 (15) (2023) 6718–6731.
[27] J. Zou, V. Rubio, J. Binner, Thermoablative resistance of ZrB_2-SiC-WC ceramics at 2400 °C, Acta Mater. 133 (2017) 293–302.
[28] E. Koch, C. Wagner, Formation of Ag_2HgI_4 from AgI and HgI_2 by reaction in the solid state, Z. Phys. Chem. 34 (1936) 317–321.
[29] R. Carter, Mechanism of solid-state reaction between magnesium oxide and aluminum oxide and between magnesium oxide and ferric oxide, J. Am. Ceram. Soc. 44 (3) (1961) 116–120.
[30] B. Yu, R.F. Davis, Self-diffusion of ^{95}Nb in single crystals of NbC_x, J. Phys. Chem. Solid. 42 (2) (1981) 83–87.
[31] H.L. Chen, S.P. Ju, T.Y. Wu, J.Y. Hsieh, S.H. Liu, Investigation of Zr and Si diffusion behaviors during reactive diffusion — a molecular dynamics study, RSC Adv. 5 (33) (2015) 26316–26320.
[32] M.M. Opeka, I.G. Talmy, J. Zaykoski, Oxidation-based materials selection for 2000 °C+ hypersonic aerosurfaces: theoretical considerations and historical experience, J. Mater. Sci. 39 (2004) 5887–5904.

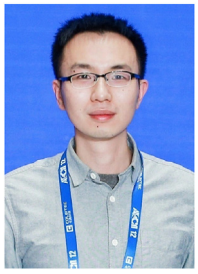

Ziming Ye obtained his Ph.D. degree in the State Key Laboratory of Powder Metallurgy at Central South University. Now, He worked as an assistant research fellow at Nanchang University. His current research is focused on the ablation mechanism of multicomponent ultra-high temperature ceramic matrix composite (UHTCMCs).

Yi Zeng is a professor and a doctoral supervisor in the State Key Laboratory of Powder Metallurgy at Central South University. His main research interests include the design and fabrication of ultra-high temperature ceramic matrix composite (UHTCMCs), the ablation and oxidation mechanism of UHTCMCs.

Xiong Xiang is a professor and a doctoral supervisor in Central South University, and a Distinguished Professor of Changjiang Scholars. He has long been engaged in aerospace new materials research and application development, with a focus on C/C composite materials, ultra-high temperature ceramic matrix composite (UHTCMCs), powder metallurgy materials and other novel materials preparation technologies.